IVYSPRING INTERNATIONAL PUBLISHER

Theranostics

2016; 6(3): 404-417. doi: 10.7150/thno.13478

Research Paper

A Multifunctional Theranostic Nanoagent for Dual-Mode Image-Guided HIFU/Chemo- Synergistic Cancer Therapy

Nan Zhang[1*], Xiaojun Cai [2*], Wei Gao [1], Ronghui Wang [1], Chunyan Xu [1], Yuanzhi Yao [1], Lan Hao [1], Danli Sheng [1], Hangrong Chen [2✉], Zhigang Wang [1✉] , Yuanyi Zheng [1✉]

1. Second Affiliated Hospital of Chongqing Medical University & Chongqing Key Laboratory of Ultrasound Molecular Imaging, Chongqing, 400010, China.
2. State Key Laboratory of High-Performance Ceramics and Superfine Microstructure, Shanghai Institute of Ceramics, Chinese Academy of Sciences.

*Nan Zhang and Xiaojun Cai are co-first authors who contributed equally to this study.

✉ Corresponding authors: Prof. Hangrong Chen, Yuanyi Zheng and Zhigang Wang are co-corresponding authors. Second Affiliated Hospital of Chongqing Medical University & Chongqing Key Laboratory of Ultrasound Molecular Imaging, 74 Linjiang Road, 400016, Chongqing, China Tel: 86-023-63693709 E-MAIL: zhengyuanyi@cqmu.edu.cn.

Received: 2015.08.06; Accepted: 2015.12.09; Published: 2016.01.20

Abstract

High-intensity focused ultrasound (HIFU) is deemed to be a promising noninvasive therapeutic modality for cancers as well as non-neoplastic diseases. However, the accuracy of the technique in the diagnosis and treatment of tumors remains unsatisfactory. HIFU, when combined with multifunctional synergistic agents (SAs), has the potential to be of greater diagnostic and therapeutic efficacy. Here we describe a smart and multifunctional hollow mesoporous Prussian blue (HMPBs) theranostic nanoplatform, the hollow structure of which is capable of encapsulating doxorubicin (DOX) and perfluorohexane (HMPBs-DOX/PFH). In vitro and in vivo studies validated that HMPBs-DOX/PFH can be used as an amplifiable dual-mode imaging contrast agent, which can simultaneously enhance ultrasound (US) and photoacoustic (PA) imaging for guiding and monitoring tumor therapy. When exposed to HIFU, this versatile HMPBs-DOX/PFH agent could increase the cavitation effect and use lower HIFU intensity to achieve coagulative necrosis. Furthermore, it significantly accelerated the release of DOX thereby enhancing chemotherapeutic efficacy and avoiding systemic side effects of the drug. Such a novel theranostic nanoplatform is expected to integrate dual-mode guided imaging with greater therapeutic efficacy and fewer side effects and is very promising for the noninvasive synergistic tumor therapy.

Key words: Hollow mesoporous Prussian blue, Phase transformation, Photoacoustic imaging, High-intensity focused ultrasound, Theranostics.

1. Introduction

High-intensity focused ultrasound (HIFU) technique has the potential for accurate image-guided ablation therapy and site-specific drug release following focused ultrasound (FUS) triggering [1]. It is considered to be a promising noninvasive therapeutic modality for non-neoplastic diseases such as uterine fibroids and various cancers including liver, pancreatic, kidney, and prostate [2-3]. It is therefore increasingly being used for the treatment of superficial tumors [4-5]. However, the technique has limitations that hinder its broad application. Although ultrasound imaging is the most common imaging technique for guiding HIFU therapy in the great majority of clinical therapies [6-7], its inadequate accuracy and low image contrast restrict noninvasive localization and treatment evaluation [8]. Furthermore, the release of high-focused acoustic power during treatment could damage normal tissue through the ultrasound

propagation path causing severe side effects (transient pain, skin burns, nerve injury) [9-10]. Thus, obtaining higher therapeutic efficacy with lower therapeutic power has remained a challenge in HIFU therapy.

Photoacoustic imaging (PA) is a promising nonionizing and noninvasive biomedical imaging system that can overcome the limitations of current ultrasound imaging systems. It simultaneously combines sensitive optical contrast with high ultrasonic resolution to precisely monitor and evaluate the process of thermal therapeutics [11-12]. The penetration depth of PA imaging in tissue-mimicking phantoms and biological tissues exceeds 5 cm thus satisfying the imaging requirements for superficial tumors. It is known that, unlike single-mode imaging, dual-mode imaging can integrate the individual strengths of medical imaging to detect tumors early and accurately [13-15]. To further promote therapeutic efficacy, several HIFU synergistic agents (SAs), such as organic microbubbles, organic nanoemulsions and inorganic nanoparticles, have been successfully fabricated. These SAs increase the ultrasonic cavitation effect by changing the acoustic environment within the tumor thereby boosting energy deposition and enhancing the efficacy and safety of HIFU therapy [16-18]. Even so, organic contrast agents have the disadvantages of extremely large particle size and low biostability, which prevent them from permeating tumor tissues [19-20]. Furthermore, microbubbles may impair the focusing of HIFU beam in tissues that can result in damage to prefocal tissues and shielding of the original targeted focus [21]. Due to their toxicity and limited biocompatibility/degradability, inorganic nanoparticles would be difficult to use in clinical practice [22-23]. In recent years, organic/inorganic hybrid nanoparticles have been designed and developed as dual-mode nanoplatforms, combining the advantages of both inorganic and organic contrast agents [24]. However, such combinations typically increase the cost, complexity of fabrication and affect in vivo performance, potentially impeding their further clinical application [25-26].

Therefore, there is a critical need to develop a single-component, biocompatible/stable, dual-mode nanoplatform for enhancing a variety of imaging modalities and increasing HIFU therapeutic efficacy. With its unparalleled properties of strong absorbance in the near-infrared (NIR) region [27], Prussian blue (PB) has attracted much attention in recent years and has been cleared by the U.S. Food and Drug Administration (FDA) for the safe treatment of radioactive exposure. Dai et al. showed that PB nanoparticles (PBNPs) displayed conspicuous PA imaging in vitro and in vivo due to their superior efficiency in NIR absorption [28]. Thus, as a superior multifunctional polymer, PB can be employed as a basis for synthesizing a novel nanoplatform to optimize and intensify PA imaging, potentially yielding an important benefit for accurate diagnosis. However, because of the lack of acoustic absorption in currently developed PB nanoparticles, their further application in HIFU therapy is limited. In a recent report, Chen et al described fabrication of hollow mesoporous Prussian blue nanoparticles (HMPBs), which were used for inducing photothermal cancer ablation in a mouse tumor model via intravenous injection [29]. Because of their characteristic hollow mesoporous structure and high absorption in the NIR, HMPBs have the potential to provide sensitive and precise PA imaging and simultaneously enhance HIFU therapy. Compared with photothermal therapy, HIFU can directly deposit acoustic energy in the focal volume to raise the temperature rapidly [30] rendering it a promising modality for the treatment of deep-seated solid tumors.

In this study, we aim to construct perfluorohexane and the anticancer drug doxorubicin-encapsulated hollow mesoporous PB nanoparticles (HMPBs-DOX/PFH), which not only enable PA/ultrasound (US) dual-mode imaging but also enhance HIFU therapeutic efficacy (Figure 1). The intrinsic properties of HMPBs make it possible to deliver payloads, including perfluorohexane (PFH) and the anticancer drug doxorubicin (DOX), into targeted tumor tissues. In addition to being an efficient US contrast agent, PFH gas can be used as a synergist to enhance the therapeutic efficacy of HIFU. Furthermore, in this novel theranostic system, drug release is sensitive to both pH and HIFU triggers thereby enhancing the therapeutic efficacy of HIFU/chemo-synergistic therapy in tumors and concurrently reducing the probability of tumor recurrence. This novel nanoplatform shows promise for achieving PA/US dual-mode imaging to guide chemotherapy and enhance HIFU treatment of tumors and has a potential application in highly efficient and noninvasive cancer therapy.

2. Materials & Methods

2.1. Synthesis of HMPBs

All chemicals were of analytical grade and were used without further purification. Polyvinylpyrrolidone (PVP, K30), potassium ferricyanide ($K_3[Fe(CN)_6]$), hydrochloric acid (HCl, 36.0 %~38.0 %) and perfluorohexane (PFH, Sigma-Aldrich-Co. LLC., St. Louis, MO, US) were purchased from Sinopharm Chemical Reagent Co., Ltd. PVP (3.0 g), $K_3[Fe(CN)_6]$ (132 mg) and HCl solution (0.01 M, 40 mL) were mixed under magnetic stirring. After achieving a clear solution, the vial was placed in an electric oven at 80

°C for 24 h. Then, by centrifugation and several washes in distilled water, mesoporous Prussian blue nanoparticles (MPBs) were obtained. PVP (5 mg/mL) was added to the solution of MPBs (1 mg/mL) in a Teflon vessel under magnetic stirring. After 3 h, the solution was placed into a stainless steel autoclave in an electric oven at 140 °C for 4 h. After centrifugation, the precipitates were washed in distilled water several times. HMPBs were acquired after freeze-drying.

2.2. Preparation of PFH and drug-loaded HMPBs (HMPBs-DOX/PFH)

HMPBs were first mixed with appropriate concentrations of DOX in phosphate-buffered saline (PBS). After stirring at room temperature in the dark for 24 h, DOX-loaded HMPBs (HMPBs-DOX) were obtained by centrifugation and drying under vacuum at room temperature. The concentration of unbound DOX was measured by UV-VIS-NIR spectroscopy with absorption intensity at 485 nm. DOX drug-loading capacity was measured using the following equation:

$$\text{Loading capacity} = (\text{total DOX} - \text{unbound DOX})/\text{total HMPBs}.$$

Vacuum-dried samples of HMPBs-DOX (25 mg) were stored in 5-mL vials and were then infused dropwise with 75 μL of temperature-sensitive PFH liquid. To prevent the volatilization of PFH, the vial was capped with a rubber plug and sealed tightly with cellophane tape. The nanoplatform was then sonicated in ice water for 2 min to facilitate the loading of the PFH into a mesoporous shell and hollow core. Finally, the HMPBs-DOX/PFH was redispersed in 5 mL of deionized water under slight magnetic stirring.

2.3. Characterization of HMPBs-DOX/PFH

The morphology and size distribution of the HMPBs were estimated by a transmission electron microscope (TEM, JEM-2100F) and analyzed with TEM imaging software (Digital Micrograph, Gatan Inc.). The sizes and the zeta potentials of the nanoparticles were measured using a Laser Particle Size Analyzer System (Zeta SIZER 3000HS; Malvern, USA). To determine whether PFH could be encapsulated into HMPBs-DOX and then exhibit phase-transition behavior, HMPB-DOX/PFH particles (0.5 mg/mL) were heated with a heating panel and visualized using an inverted fluorescence microscope. UV-VIS-NIR spectroscopy was recorded on a UV-2550 Shimadzu spectroscope.

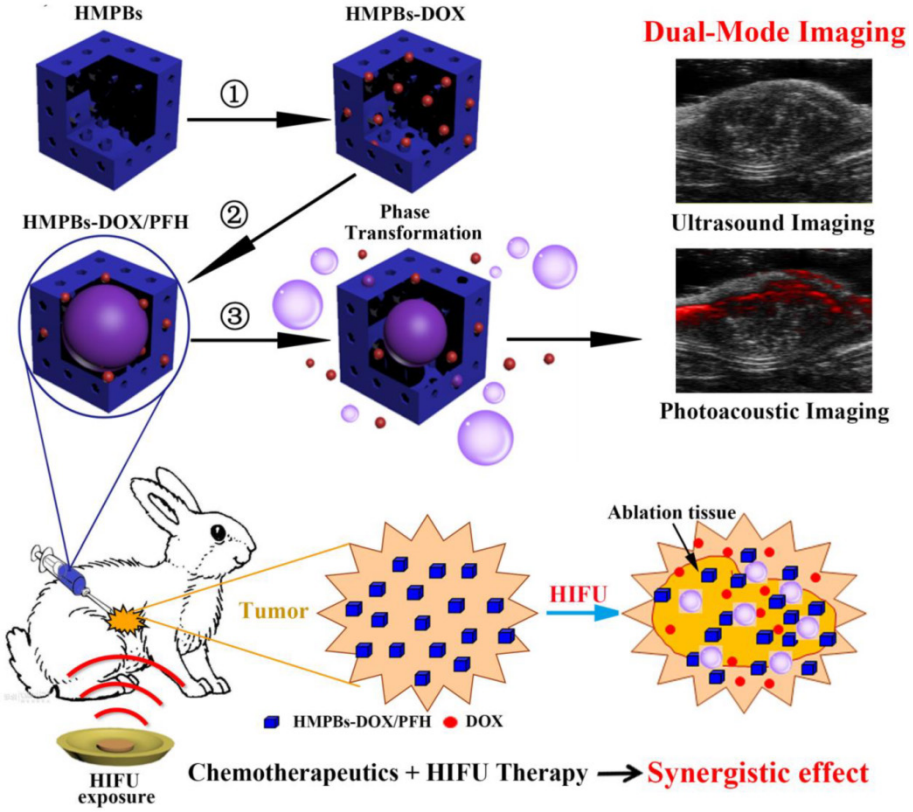

Figure 1. Schematic diagram of the smart multifunctional nanoplatform (HMPBs-DOX/PFH) for dual-mode imaging and tumor therapy. The fabrication process of HMPBs-DOX/PFH: ① doxorubicin (DOX) loading, ② temperature-sensitive liquid PFH encapsulation. After HIFU exposure, drug release and PFH bubbles generation were observed ③ This versatile nanoplatform can be detected under US and PA for dual-mode guiding and monitoring tumor therapy, as well as enhancing synergistic effect of HIFU ablation and chemotherapeutics.

2.4. The drug release behavior of HMPBs-DOX/PFH when triggered by HIFU at different pH values

The release profiles of HMPBs-DOX/PFH at different pH values with and without exposure to HIFU were investigated. Samples of the same HMPB-DOX/PFH solution were placed in 3 dialysis bags with solutions of different pH (pH 4.6, pH 6.0 and pH 7.4) that were shaken at 100 rpm. The DOX release behavior in different pH conditions was investigated using a high-performance liquid chromatography (HPLC) method for comparison. To further explore the release behavior of drug carriers after HIFU stimulation, HMPBs-DOX/PFH were first prepared using the aforementioned methods, and the samples in the 3 different pH conditions were triggered after 5 h by HIFU at 120 W for 5 s. After HIFU triggering, the samples were subsequently shaken in the shaker for 19 h, and DOX release concentrations were detected. The HIFU-triggered release and distribution of DOX were evaluated in ex vivo bovine livers. After injection of HMPBs-DOX/PFH with or without HIFU exposure (120 W for 5 s), tissues 1 cm distal from the center of the ablation area were collected for snap-frozen sections. The fluorescence intensity of the inherently fluorescent DOX was then observed with an inverted fluorescence microscope. After heating at 80 °C for 30 min, the thermostability of the DOX was analyzed using an HPLC method.

2.5. In vitro cytotoxicity of HMPBs-DOX/PFH

MB231 cells were seeded in a 96-well plate at a density of 5×10^4 cells per well at 37 °C in a 5% CO_2 atmosphere for 24 h. Wells without cells acted as blank controls. Different concentrations of HMPBs in a solution medium (400, 200, 100, 50, and 25 μg/mL) were prepared and used to replace the previous medium. After 18 h, 20 μL of MTT at a concentration of 5 mg/mL was added to each well and incubated for 4 h. After removing the medium, 150 μL of DMSO was added to each well. The absorbance of each well was measured at 490 nm with a microplate reader (EL×800 Universal Microplate Reader, BIO-TEK Instrument Inc.). For in vitro ultrasound therapy, MB231 cancer cells were incubated with different agents (saline, DOX, HMPBs-DOX, HMPBs-PFH, and HMPBs-DOX/PFH) for 18 h and then exposed to a portable ultrasound therapeutic apparatus (invented by Chongqing Medical University HIFU Institution, Chongqing, China) using a 1-MHz transducer at 2 W/cm^2 and a continuous duty cycle for 1 min, with a focal distance of 15 mm. The media were replaced with DMSO, and the cytotoxicity of each agent was measured with a microplate reader using an MTT assay.

2.6. In vitro dual-mode imaging

The function of HMPBs-DOX/PFH as a contrast agent for dual-mode imaging was evaluated in vitro using an agar gel phantom. The gel phantom was made using 2 % agar-agar (w/v) and dissolved in deionized water. An Eppendorf tube was placed in the center of the phantom to create a hole into which the HMPBs-DOX/PFH solution was deposited. The US images and the corresponding average gray value of the ROI (region of interest) for the saline control, PFH, HMPBs-DOX, and HMPBs-DOX/PFH samples under standard B-mode and contrast-mode were investigated with MyLab 90 (Esaote, Italy) using a linear probe (5-12 MHz). After the 4 agents were exposed to HIFU using 120 W for 5 s (JC 200, Chongqing Medical University, Chongqing, China), US B-mode and contrast-mode images were captured for each group. An "average gray scale" was analyzed using DFY (invented by the Institution of Ultrasound Imaging of Chongqing Medical University, Chongqing, China) to quantitatively measure the captured images. In vitro PA images of the different samples were estimated using the VEVO LASR PA imaging system (VIVO 2100, FUJIFILM Visual Sonics, Inc., USA) by following the methods described above. The HMPBs-DOX/PFH and HMPBs-DOX were placed into a rubber bag and then incubated in a water bath kettle at 65 °C, and the PA intensity variation was observed using the VEVO LASR PA imaging system.

2.7. Implantation of VX2 breast tumors

All animal experiments were approved by our animal ethics committee. New Zealand white rabbits, as recipient animals, were obtained from the Animal Center of Chongqing Medical University under protocols approved by the Institute's environmental guidelines. Tumor-bearing rabbits with a VX2 tumor in the liver were obtained from the Chongqing Key Laboratory of Ultrasound Molecular Imaging at Chongqing Medical University. All experiments and procedures were performed under complete anesthesia. Under general anesthesia by intramuscular injection with 3% pentobarbital solution (1 mL/kg), the abdomens of the rabbits were depilated with 8% Na_2S solution. In the supine position, the rabbits were routinely disinfected. After a histological section had been taken, the tumor tissues from tumor-bearing rabbits were soaked in 20 mL of Hanks' balanced salt solution. Next, the tumor was sheared into small masses of approximately 1.0 mm^3. A surgical hole was created underneath the left second nipple using a 50-mL syringe. Subsequently, one piece of tumor tissue was implanted into the hole using ophthalmological forceps. The wound was sutured after hemostasis. The skin incision was then disinfected and

covered. To prevent infection, 400,000 units of streptomycin were intramuscularly injected over the 3 days following the procedure.

2.8. In vivo dual-mode imaging

New Zealand white rabbits with detectable breast cancer were anesthetized, depilated and fixed in the supine position. Then, VX_2 tumor-bearing rabbits were intratumorally injected with saline (control) or with HMPBs-DOX/PFH (n = 6 in each group) before imaging. PA and US images were taken pre-injection, post-injection and post-HIFU exposure (120 W for 5 s). The PA average value and US average gray scale of the ROI were detected using the small-animal PA imaging system.

2.9. Ex vivo and in vivo experiments by HIFU exposure

Ex vivo degassed bovine livers, 10 cm × 8 cm × 6 cm in size, were prepared and placed in a container filled with degassed water in the HIFU system. Saline, HMPBs, DOX, HMPBs-DOX, HMPBs-PFH, or HMPBs-DOX/PFH (0.2 mL, 6 mg/mL) was directly injected into the bovine livers. Immediately after the injections, HIFU ablation (120 W for 5 s, 150 W for 5 s, or 180 W for 5 s) was performed at the injection site. High echoes were acquired, and pre- and post-ablation gray scale values were recorded using GrayVal 1.0 software (Chongqing Haifu Technology, Chongqing, China). The maximum length (L, mm), width (W, mm) and depth (D, mm) of the coagulated liver tissues were measured using a calibrated scale, and the related ablation volumes (V, mm^3) in the degassed bovine livers were calculated by the following equation: $V = \pi/6 \times L \times W \times D$. The exposure temperature was recorded with a temperature-sensing needle.

The 48 rabbits in the study were randomly divided into 8 groups: saline (n = 6), HIFU (120 W, 5 s) combined with saline (n = 6), DOX (n = 6), HMPBs-PFH (n = 6), HIFU (120 W, 5 s) combined with HMPBs-PFH (n = 6), HMPBs-DOX/PFH (n = 6), HIFU (120 W, 5 s) combined with HMPBs-DOX/PFH (n = 6), and HIFU (400 W, 5 s) combined with saline (n = 6). The rabbits received an intratumoral injection of 0.2 mL normal saline, DOX, HMPB-PFH, or HMPB-DOX/PFH solution into the breast tumors at 3, 6, 9, or 12 dots, respectively, and were massaged for 1 min. The US images and gray scale were recorded pre-injection and post-injection and were analyzed using GrayVal 1.0 software. Next, the saline + HIFU (120 W), HMPBs-PFH + HIFU, and HMPBs-DOX/PFH + HIFU groups were exposed to HIFU at an acoustic power of 120 W for 5 s, while the saline + HIFU (400 W) group was exposed to HIFU at 400 W for 5 s. During HIFU treatment, the ablation effects were assessed using diagnostic US images in real-time. After HIFU ablation, the tumor volumes of all rabbits on days 1, 3, 5, 7, 9, 11, 13 and 15 were recorded. After euthanasia, the breast tumors of all rabbits were immediately removed. The tumor resection range was 1 cm^3 in a region center around the ablated zone. Hematoxylin and eosin (HE) staining was performed for pathological examination. An immunohistochemical examination of the targeted tissue was performed to evaluate the proliferation of these tissues; it included a terminal deoxynucleotidyl transferase-mediated dUTP-biotin nick end-labeling assay (TUNEL) and staining for proliferating cell nuclear antigen (PCNA). The proportion of positive cells among the total number of cells was assessed by reading 5 random fields at 400× magnification.

3. Results and Discussion

3.1. Characterization of HMPBs-DOX/PFH.

HMPBs were prepared by selective protection and etched by using PVP as the protective agent and hydrochloric acid as the etching agent. As shown in Figure 2a, the HMPBs had uniform size and good monodispersion, showing a cube-like morphology with a hollow mesoporous structure. The apparent structural characteristics of HMPBs, with a large cavity and a mesoporous shell, were further evidenced in representative high-magnification TEM images (upper left in Figure 2b). The corresponding element mapping (Figure 2b) confirmed the successful creation of an inner cavity in the HMPBs. The average particle size and average zeta potential of the nanoplatform were 269 nm and about -33.7 mV, respectively (Figure 2c-d). With its hollow mesoporous structure and excellent biostability, HMPBs can serve as ideal carriers of anticancer drugs and/or other molecules. As a model drug, DOX was successfully loaded into HMPBs, as verified by UV-VIS-NIR spectroscopy and the inset digital photographs of DOX solutions before and after interaction with HMPBs (Figure 2e). Interestingly, the drug-loading capacity can be as high as 1,650 mg/g, suggesting that the local chemotherapeutic effect can be substantially strengthened while avoiding undesirable systemic side effects.

We also investigated whether PFH could be efficiently encapsulated into HMPBs. As shown in Figure 2f, digital photographs of a transparent and well-dispersed HMPB-DOX/PFH solution in PBS demonstrated that the poorly soluble PFH molecules could be satisfactorily encapsulated into HMPBs. The Tyndall phenomenon was apparent, showing that HMPBs-DOX/PFH had excellent dispersibility. In

comparison, an obviously phase-separated mixture was observed for the same concentration of free PFH in PBS. To further confirm the successful loading of PFH into HMPBs, HMPBs-DOX/PFH were heated from 25 °C to 65 °C and observed with an inverted fluorescence microscope according to the temperature-responsive property of PFH (liquid-gas phase transition temperature of 56 °C). As shown in Figure 2 g-h, there were no obvious bubbles generated below 56 °C, while a large number of bubbles were generated and visualized after the temperature reached 63 °C during the liquid-gas phase transition of PFH, indicating that the PFH was successfully encapsulated into HMPBs. Furthermore, small adjacent microbubbles were able to swell and further merge into larger micrometer-sized bubbles that could alter the acoustic environment and induce the cavitation effect to enhance the performance of ultrasound imaging and HIFU therapy. The HMPBs-DOX/PFH nanosystem exhibited greater stability (the PFH core is biologically stable, inert and well tolerated with a boiling point of 56 °C) in circulation at physiological temperatures [31]. When the HMPBs-DOX/PFH nanosystem was transported into the targeted tumor, under the site-specific exposure of HIFU, the microscale gas bubbles were locally released only into the tumor to enhance its imaging and therapeutic efficacy. Thus, this nanosystem was stable and the targeted releasing of microscale gas bubbles could avoid the possibility of aeroembolism in the pulmonary vein resulting in respiratory problems. In UV-VIS-NIR spectra, HMPBs and HMPBs-DOX/PFH showed strong absorbance in the NIR region (from 600-900 nm, Figure 2i). This indicates that, similar to unloaded HMPBs, the potential application of HMPBs-DOX/PFH for PA imaging is promising.

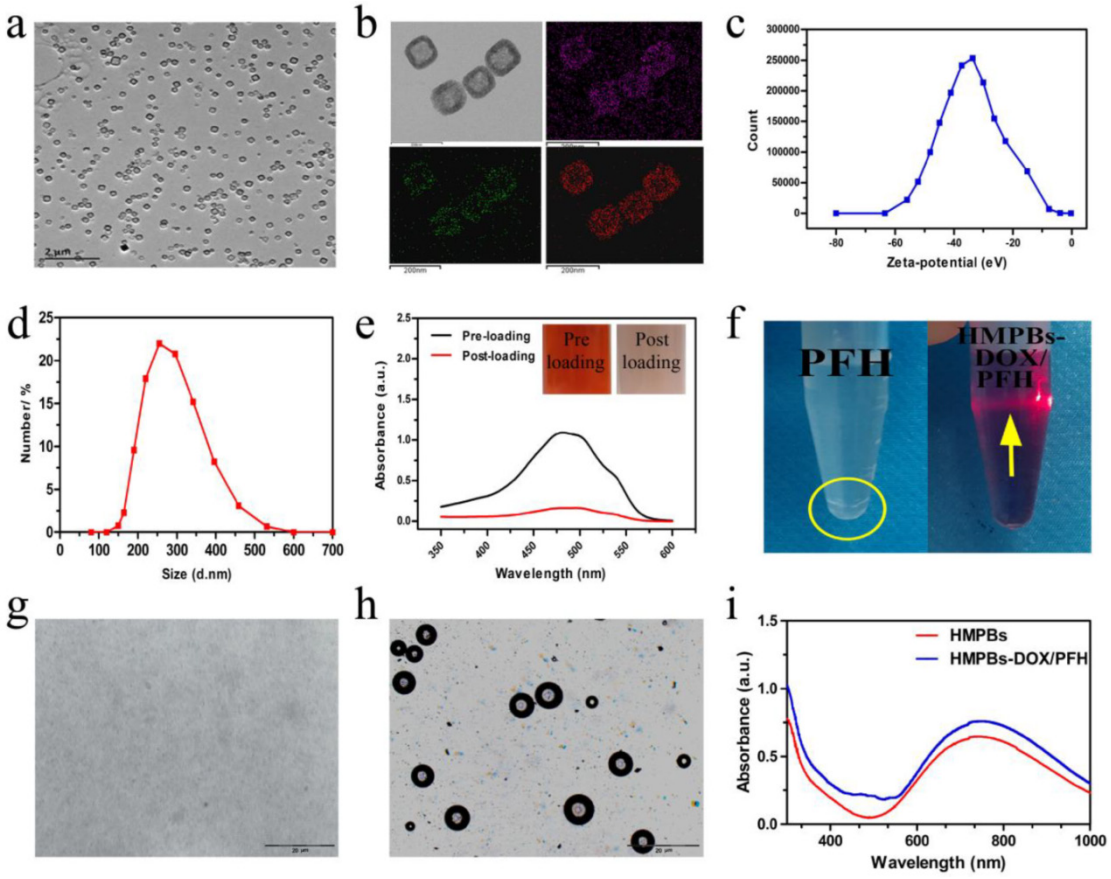

Figure 2. Characterizations of HMPBs-DOX/PFH. (a) A TEM image of HMPBs-DOX/PFH. **(b)** A high magnification TEM image of HMPBs-DOX/PFH (upper left).The corresponding elemental mappings of HMPBs: carbon, nitrogen and iron (upper right, lower left and right, respectively). **(c-d)** The size distribution and Zeta potentials of HMPBs-DOX/PFH were measured by dynamic light scattering technique. **(e)** The UV-vis-NIR spectroscopy of DOX solutions before and after interaction with HMPBs (inset: the representative photos of DOX solution before (left) and after interaction with HMPBs (right)). **(f)** Digital photos of free PFH and HMPBs-DOX/PFH at the same PFH concentration in PBS (yellow circle indicates the phase-separation of PFH from PBS, yellow arrow indicates tyndall phenomenon). **(g-h)** Inverted fluorescent microscope images of HMPBs-DOX/PFH at room temperature **(g)**, heated at 63 °C for 10 s **(h)**. **(i)** The UV–vis–NIR spectroscopy of HMPBs and HMPBs-DOX/PFH.

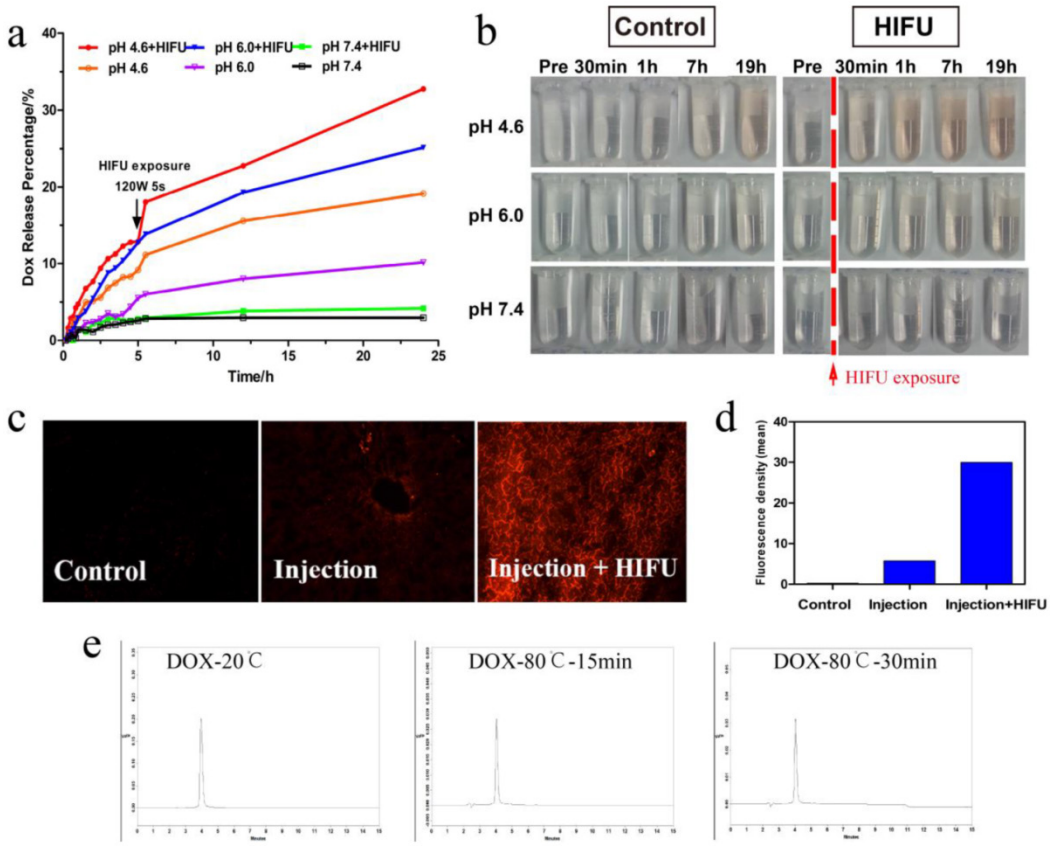

Figure 3. In vitro and ex vivo bovine liver HIFU/pH-dual controlled release of DOX. (a) The DOX release curves at different pH levels with or without HIFU exposure. An obvious rise was exhibited at 5 h for HIFU exposure. **(b)** Digital photos of samples at different time-points (pre exposure, post exposure 30 min, 1 h, 7 h, 19 h) without HIFU exposure (left) and with HIFU exposure (right) in PBS. HIFU exposure group would markedly enhance DOX release against control group due to the solution became redder. **(c)** DOX fluorescence microscope images of ex vivo bovine liver were obtained by Inverted fluorescence microscope. **(d)** The quantitative analysis of DOX fluorescence intensity. **(e)** High Performance Liquid Chromatography (HPLC) images of DOX aqueous solution (20 °C), DOX aqueous solution (80 °C, 15 min) and DOX aqueous solution (80 °C, 30 min).

3.2. Doubly responsive triggered drug-release profile

Controlled-release systems have the potential to enable better regulation of drug release over time, to assist drugs in crossing physiological barriers and to guide drugs to the desired site of action while minimizing drug exposure elsewhere in the body [32]. We investigated the drug-release profile of HMPBs-DOX/PFH when stimulated by HIFU and pH. As shown in Figure 3a, drug release greatly depends on the pH value. Only a small amount of drug was released at pH 7.4 (5.12 %) after 48 h. When the pH values were reduced to 6.0 or 4.6, the drug-release percentages increased to 24.55% and 45.31% respectively, after 48 h. As shown in Figure 3a, a substantially higher DOX release rate was observed with the decreasing of pH value, which was also reported by other author [29]. This significant phenomenon can be attributed to two factors: one is the electrostatic interaction and strong coordinative bonding between HMPBs (negatively charged) and DOX (positively charged) were weakened at reduced pH values; the other is the higher solubility of DOX at lower pH values [29, 33-34]. Moreover, there was a dramatic and immediate increase in the drug release percentage at all pH values with additional HIFU exposure after 5 h. This effect was especially apparent at pH 4.6 (from 12.88 % to 18.05 %), indicating that release of the DOX in the HMPBs-DOX/PFH could be triggered by HIFU exposure.

The digital photographs of drug-release solutions at different pH values over time, shown in Figure 3b, were consistent with the results of the drug-release profiles. To detect the effect of the drug release on biological tissues, HMPB-DOX/PFH solution was injected into bovine livers. As shown in Figure 3c-d, the red fluorescence signal (29.36 IU/mL) from the DOX molecules was distinctly higher (5.832 IU/mL) under HIFU exposure than without HIFU stimulus, indicating that drug release can be controlled by HIFU stimulation. These results suggest that ultrasound waves could trigger the drug release from a variety of nanocarriers through the thermal effects as well as the cavitation effects. Similar to NIR irradiation, focused ultrasound energy could be sufficient to induce thermal phenomenon leading to cell death by coagulative necrosis. It also increases the

intracellular and intercellular concentration of nanoagents that can improve the efficacy of anticancer drugs [35]. Most importantly, PFH has the potential ability to enhance acoustic cavitation, which can temporarily induce destabilization of nanocarriers resulting in drug release. It can also increase the permeability of cell membranes for increased uptake and release of the anticancer drugs in the tumor site [36]. Accordingly, we found a significantly higher drug release in HMPBs-DOX/PFH than in HMPBs-DOX (Figure S1, Supporting Information).

We also validated the thermostability of DOX at high temperatures. As shown in Figure 3e, the HPLC traces of aqueous DOX solution after incubation at 80 °C for 15 min or 30 min were the same as at 20 °C, indicating that the drug properties of DOX are preserved after HIFU stimulus. According to the aforementioned in-vitro and ex-vivo experiments, this novel system based on HMPBs-DOX/PFH can enable doubly responsive drug release based on pH and HIFU stimulus, thus giving HMPBs-DOX/PFH significant potential for synergistic chemotherapy and HIFU therapy against tumors.

3.3. *In vitro* cytotoxicity of HMPBs-DOX/PFH

The outstanding controlled drug-release properties of HMPBs-DOX/PFH prompted us to investigate the *in vitro* therapeutic efficacy in more detail. The cytotoxicity of HMPBs was confirmed using MB231 breast cancer cells that were incubated with different HMPBs concentrations. HMPBs treatment permitted a high cell viability of approximately 92%, even at a high concentration of 400 μg/mL (Figure S2, Supporting Information), indicating that HMPBs are biologically safe and promising nanoplatforms. An MTT assay was employed to quantitatively measure cell viabilities after incubating MB231 cancer cells with saline, DOX, HMPBs-DOX, HMPBs-PFH, or HMPBs-DOX/PFH with or without FUS exposure (1 MHz transducer at 2 W/cm^2 for 60 s). The free DOX group (23.6 %) showed higher toxicity than the HMPBs-DOX group (14.6%) or the HMPBs-DOX/PFH group (13.7 %) due to the limited DOX release from HMPBs. The HMPBs-DOX + FUS group had a cell mortality rate of 34.0 %, while 49.3 % cell mortality was observed in the HMPBs-DOX/PFH + FUS group (Figure S3, Supporting Information). Corresponding to in vitro drug release study, US-induced thermal effects and further bubble cavitations are probably the main mechanisms of cytotoxicity, as they can result in cytoclasis or cell necrosis. These mechanisms also explain why the viability of cells without nanoparticles but with the same FUS exposure was relatively high. These in vitro results indicate that HMPBs-DOX/PFH can be the desirable HIFU SAs for enhancing therapeutic efficacy and for decreasing lesions in neighboring, unexposed tissues.

3.4. *In vitro* and *in vivo* dual-mode imaging of HMPBs-DOX/PFH

We explored the imaging capabilities of PFH bubbles, whose generation is temperature-sensitive in HMPBs-DOX/PFH, for tumor diagnosis. B-mode and contrast-enhanced US (CEUS) imaging were performed on four different groups (saline, PFH, HMPBs-DOX and HMPBs-DOX/PFH) with or without HIFU stimulus. As shown in Figure 4a, there were no obvious changes in B-mode or CEUS images in the saline group and HMPBs-DOX group. In the other two groups with PFH, but without or with HIFU stimulus, there were obvious changes to the B-mode and CEUS images; these changes were ascribed to the liquid-gas phase transition of PFH by HIFU stimulus. Particularly in the HMPBs-DOX/PFH group, the echo and CEUS intensity increased from 14.33 to 113 and from 1 to 95, respectively (Figure 4b-c).

We also investigated the PA performance of all four groups using the Vevo LAZR PA imaging system. No obvious differences in the PA imaging before and after HIFU exposure were observed in either the saline or the PFH groups. However, because of the strong absorption in the NIR range, the HMPBs-DOX and HMPBs-DOX/PFH groups showed markedly enhancement in PA imaging (Figure 4d). These observations are consistent with other studies of PB [28]. HMPBs-DOX/PFH showed the ability to be both a US and PA imaging contrast agent (Figure 4e-f). We also surprisingly found that the PA intensity of the HMPBs-DOX/PFH group (16.35 ± 1.046 a.u.) was higher than that of the HMPBs-DOX group (11.144 ± 2.347 a.u.) after HIFU exposure. This difference was ascribed to the contrast enhancement from the increased temperature and PFH gas generated by the HIFU stimulus (Figure 4f). To confirm whether the PA intensity enhancement was from PFH-transformed gas, US and PA imaging of the HMPBs-DOX/PFH, HMPBs-DOX and HMPBs groups were observed in real-time. The US and PA imaging showed no distinct change between the HMPBs-DOX and HMPBs groups. However, as the heating time increased, the echo intensity value of the B-mode images in the HMPBs-DOX/PFH group rapidly increased for the initial 20 s and then stabilized after 20 s (Figure S4, Supporting Information). Interestingly, as the heating time increased, the PA signal intensity also kept increasing during the heating process, from 1.067 ± 0.467 a.u. at the beginning to 1.590 ± 0.315 a.u. after heating for 100 s. While there was no obvious change in HMPBs group (from 0.766 ± 0.375 a.u. to 0.794 ± 0.361 a.u.) and HMPBs-DOX group (from 0.814 ± 0.341

a.u. to 0.775±0.395 a.u.). At a high temperature, the temperature-responsive PFH could generate gas microbubbles via its liquid-gas phase transition, which could enhance the real-time US and PA imaging [12] (Figure S5, Supporting Information). Based on the link between PA/US imaging and temperature, we hypothesize that HMPBs-DOX/PFH are stimulated by HIFU, whose high temperature can also enhance US and PA imaging. Thus, we have demonstrated that HMPBs-DOX/PFH could considerably enhance the therapeutic efficacy of HIFU, indicating its great potential as a contrast agent to further improve US and PA imaging.

Based upon the excellent results of PA/US imaging performance *in vitro*, the imaging studies were also performed *in vivo* by directly injecting HMPB-DOX/PFH solution into the tumor tissue (subcutaneously transplanted VX_2 tumors; n = 6). Subsequently, the echo intensity of the tumors increased from 21.33 ± 3.512 to 37.33 ± 4.726. Due to the strong absorbance of the HMPBs in the NIR range, the PA signal intensity of each tumor after injection was much stronger than the pre-injection value increasing from 0.274 ± 0.101 a.u. to 1.218 ± 0.094 a.u. (Figure 4g). Next, the HMPB-DOX/PFH-injected tumors were exposed to HIFU stimulus at 120 W for 5 s. The echo intensity of each tumor increased three-fold over the pre-injection value (Figure 4h); this difference was attributed to the bubbles generated by the liquid-gas phase transition of PFH by the HIFU stimulus. Interestingly, we note that the PA signal intensity further increased after HIFU exposure (Figure 4i), which is consistent with the in vitro results and indicates that HIFU can enhance the US and PA imaging capacities of HMPBs-DOX/PFH.

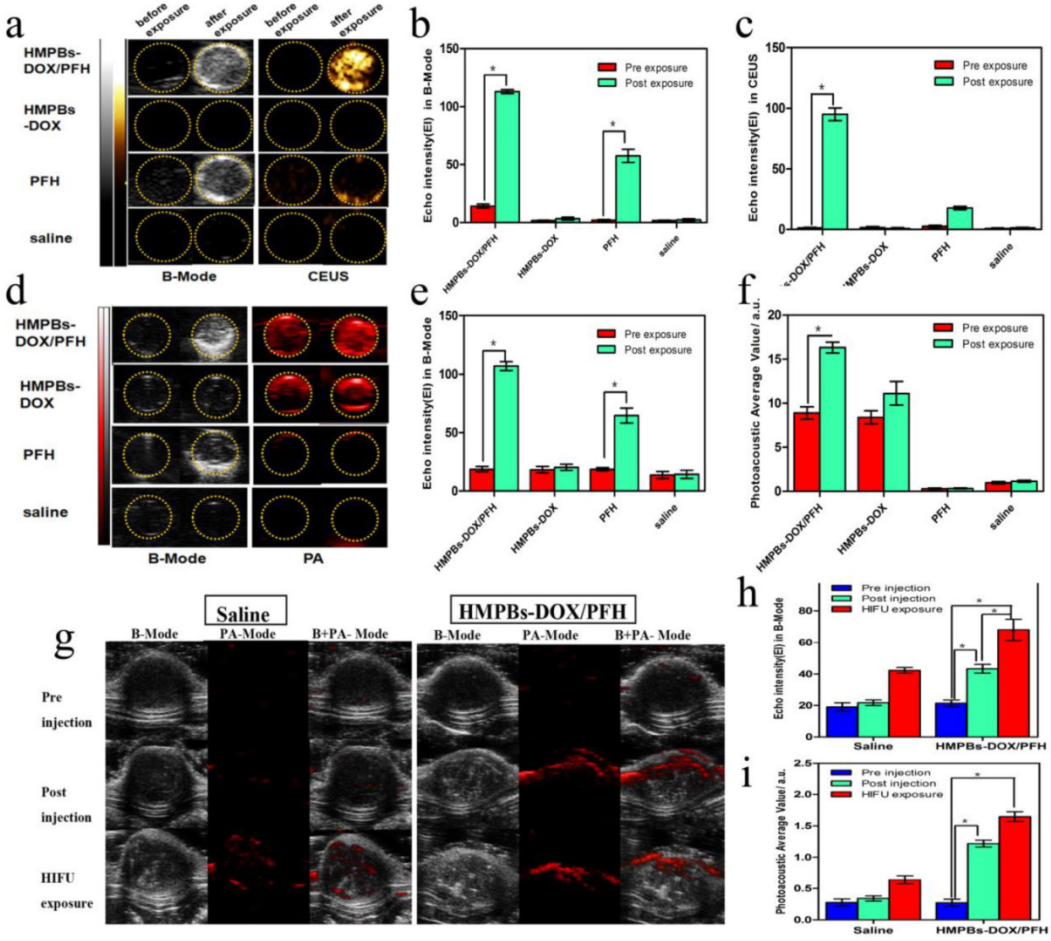

Figure 4. Dual-mode imaging in vitro and in vivo experiments. (a) B-Mode and contrast enhanced ultrasound (CEUS) imaging of particles before and after HIFU exposure in vitro (gel model) for HMPBs-DOX/PFH (top row), HMPBs-DOX (second row), PFH (third row) and saline only (bottom row). **(b-c)** Echo Intensity (EI) in B-Mode and CEUS before and after HIFU exposure. Echo intensity value of B-mode in HMPBs-DOX/PFH group was five times higher than other three groups. Similarly, echo intensity value of CEUS in HMPBs-DOX/PFH group was almost ten times higher than other three groups. **(d)** B-Mode and PA-Mode imaging of particles before and after HIFU exposure in vitro (gel model) for the same groups. **(e-f)** Echo Intensity (EI) in B-Mode and photoacoustic average value before and after HIFU exposure. The PA intensity value of post-exposure (16.35 ± 1.046 a.u.) was approximately twice as high as the one of pre-exposure (8.901 ± 1.197 a.u.) in HMPBs-DOX/PFH group. **(g)** B-Mode and photoacoustic imaging of saline and HMPBs-DOX/PFH before and after HIFU exposure in vivo for pre-injection (top row), post-injection (middle row) and after HIFU exposure (bottom row). **(h-i)** Echo Intensity (EI) in B-Mode and photoacoustic average value before and after HIFU exposure.

Because of their distinctive hollow mesoporous structure, the prepared HMPBs can be loaded with both anticancer drugs (e.g., DOX) and phase-change materials (e.g., PFH). When exposed to HIFU, the accumulated HMPBs-DOX/PFH within the tumor can transform the focused ultrasound into heat, causing PFH bubbling with increasing temperature. On one hand, the resulting bubbles act as a US contrast agent to sensitize the US imaging signal and enhance the HIFU therapeutic efficacy. On the other hand, the HMPBs show high intrinsic NIR absorption properties that allow desirable PA imaging. Therefore, this novel single component, multifunctional nanoplatform shows high NIR absorption for PA imaging and PFH bubbles for enhanced US imaging thereby improving accuracy of tumor diagnosis.

3.5. Combined chemotherapy and HIFU ablation treatment.

Because of the superior in vitro PFH phase-transformation performance, we further investigated the ablation therapeutic efficiency of the HMPBs. First, because of the changed gray scale value at the focus point in real-time B-mode US imaging and the related quantitative necrosis volume, coagulative necrosis was studied ex vivo with degassed bovine livers, as shown in the 3D schematic illustration in Figure 5a. Following injection with saline, HMPBs, DOX, HMPBs-DOX, HMPBs-PFH or HMPBs-DOX/PFH, the necrotic volumes of ablated bovine livers were measured to evaluate the ex vivo HIFU synergistic effect. As expected, the necrotic volumes and gray scale areas of the HMPB-PFH and HMPB-DOX/PFH groups (shown in the two right-hand rows of Figure 5b-c) were larger than those of the other four groups after HIFU exposure at different power levels (120, 150 and 180 W for 5 s). As shown in Figure 5d, the related quantitative necrotic volume in the HMPBs-DOX/PFH group was at least 10 times larger than the volume in the saline group at the same power. Notably, the necrotic volume with HMPBs-DOX/PFH (i.e., 120 W, 5 s: 150.817 ± 41.281 mm^3) was significantly larger than with HMPBs-DOX (120 W, 5 s: 17.7 ± 4.769 mm^3) or with the saline control (120 W, 5 s: 2.18 ± 0.745 mm^3). This suggests strongly that PFH encapsulated in HMPB nanocarriers could act as phase-change agents and generate microbubbles in situ during HIFU exposure thereby playing a significant role in enhancing the ablation effect. The appearance of microbubbles in a region of tissue dramatically alters its acoustic impedance, causing reflection of the incident sound wave and increasing sound intensity in the region proximal to the focal volume [37]. Acoustic cavitation induced by PFH could help achieve the desired therapeutic effects using much lower intensities than those currently employed in most clinical systems. To verify that these intensity parameters could achieve the vaporization temperature of PFH, the exposure temperatures at 120, 150, and 180 W were detected using a temperature-sensing needle ex vivo (Figure 5e). We noted that the exposure temperatures with these intensity parameters, even at 120 W, reached the vaporization temperature of PFH to permit the phase transition. The resultant mechanical and thermal effects from HIFU and the thermally induced PFH bubble cavitations are probably responsible for the increased ablation effect.

We also investigated the in vivo therapeutic efficacy of HMPB-DOX/PFH-induced HIFU/chemotherapy for cancer treatment. Seven groups (n = 6) of rabbits with VX_2 xenografts of breast cancer were used. We employed a power intensity of 120 W in the in-vivo experiment which, compared to 150 and 180 W, represented a low HIFU intensity that could produce sufficient therapeutic effects while avoiding unnecessary damage to the adjacent tissue. As shown in the digital photographs (Figure 6a), the tumor volumes of the HMPB-PFH + HIFU group apparently decreased, while the tumor volumes of the saline group significantly increased in the 15 days following treatment. However, while such a treatment demonstrates a noticeable effect on tumor growth, it failed to regress or to completely eliminate the tumor. When the tumor was subjected to the synergistic treatment with HMPBs-DOX/PFH and HIFU exposure, there was a significant decrease in the tumor volume The contrast enhancements in the gray scale was obvious when HMPBs-DOX/PFH with HIFU ablation was used at 120 W for 5 s (181) compared to the gray scale using saline (142). This indicates a highly increased necrotic effect of HMPBs-DOX/PFH on malignant tumors (Figure 6b). As expected, the tumor volume in the HMPBs-DOX/PFH + HIFU group (168.2 ± 7.55 %) was lower than that in other groups (e.g., saline: 1603.313 ± 67.261 %) 15 days after the treatment (Figure 6c). The result is similar with the report by Chen under the exposure of NIR [29]. Different with his research, we have employed HIFU treatment method, which can not only treat superficial lesion, but also be applicable in deep-site tumor (Figure S6). In addition, HIFU therapy depends on three most important mechanisms: heat generation, acoustic cavitation, and mechanical effect. These mechanisms have potential ability to enhance ablation effect and increase drug release in the tumor site.

To further confirm the synergistic effect of combining HIFU ablation with chemotherapy, we created another a HIFU-only group that was exposed to HIFU at 400 W for 5 s. We observed that the tumor volume

after high-intensity (400 W for 5 s) HIFU exposure in this group was significantly larger than that in the HMPB-DOX/PFH + HIFU group after 15 days. This result indicates that HMPBs-DOX/PFH could induce an effective and sufficient treatment whose therapeutic efficiency was superior to the high-intensity HIFU at 400 W, thus avoiding damage to adjacent normal tissue by excessive HIFU exposure. Thus, HMPBs-DOX/PFH nanosystem generated a range of acoustic cavitation effects and thermal mechanisms that can enable rapid and highly localized thermal ablation, as well as promote the efficiency of site-specific drug release for achieving synergistic HIFU/chemotherapy.

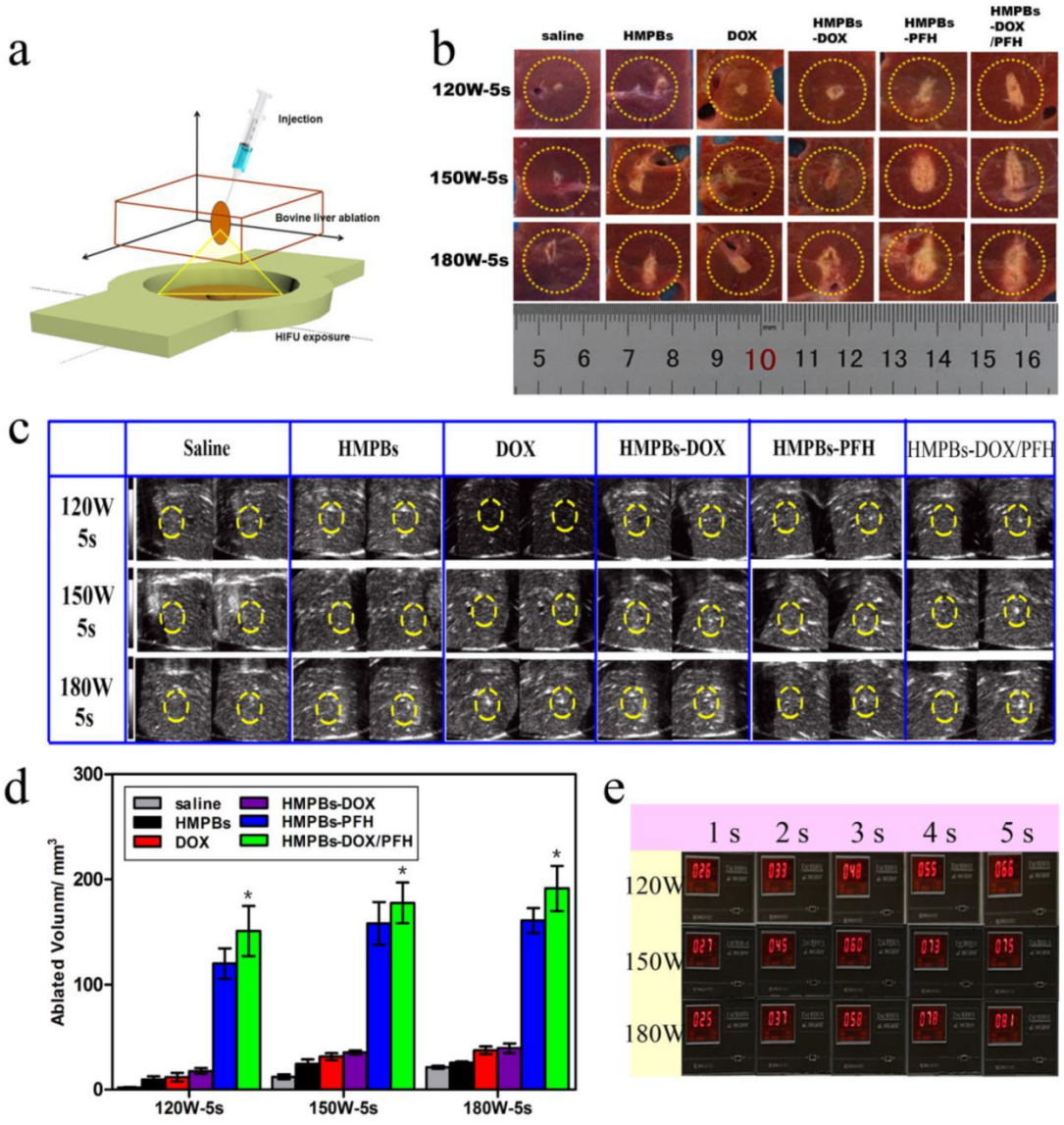

Figure 5. Ex vivo HIFU synergistic effect assessment. (a) Schematic 3D illustration of ablation process on bovine livers in vitro. **(b)** Digital photos of ablated bovine livers exposed to HIFU at 120 W, 150W and 180 W for 5 s after injection of 0.3 mL saline control, HMPBs, DOX, HMPBs-DOX, HMPBs-PFH and HMPBs-DOX/PFH. **(c)** Typical in vitro B-mode ultrasound images before and after HIFU exposure on degassed bovine livers at 120 W, 150W and 180 W for 5 s. **(d)** The corresponding necrotic volume after injection of the same samples. The necrotic volume in HMPBs-DOX/PFH group was higher than that in the other four groups ($p<0.05$). However, there is no significant difference between HMPBs-DOX/PFH group and HMPBs-PFH group ($p>0.05$). The necrotic volume of HMPBs-DOX/PFH group is at least ten times larger than the volumes of saline group at the same power. **(e)** Ex vivo temperature were observed by thermodetector in order to illustrating HMPBs-DOX/PFH can generate PFH bubbles using these HIFU ablation parameters.

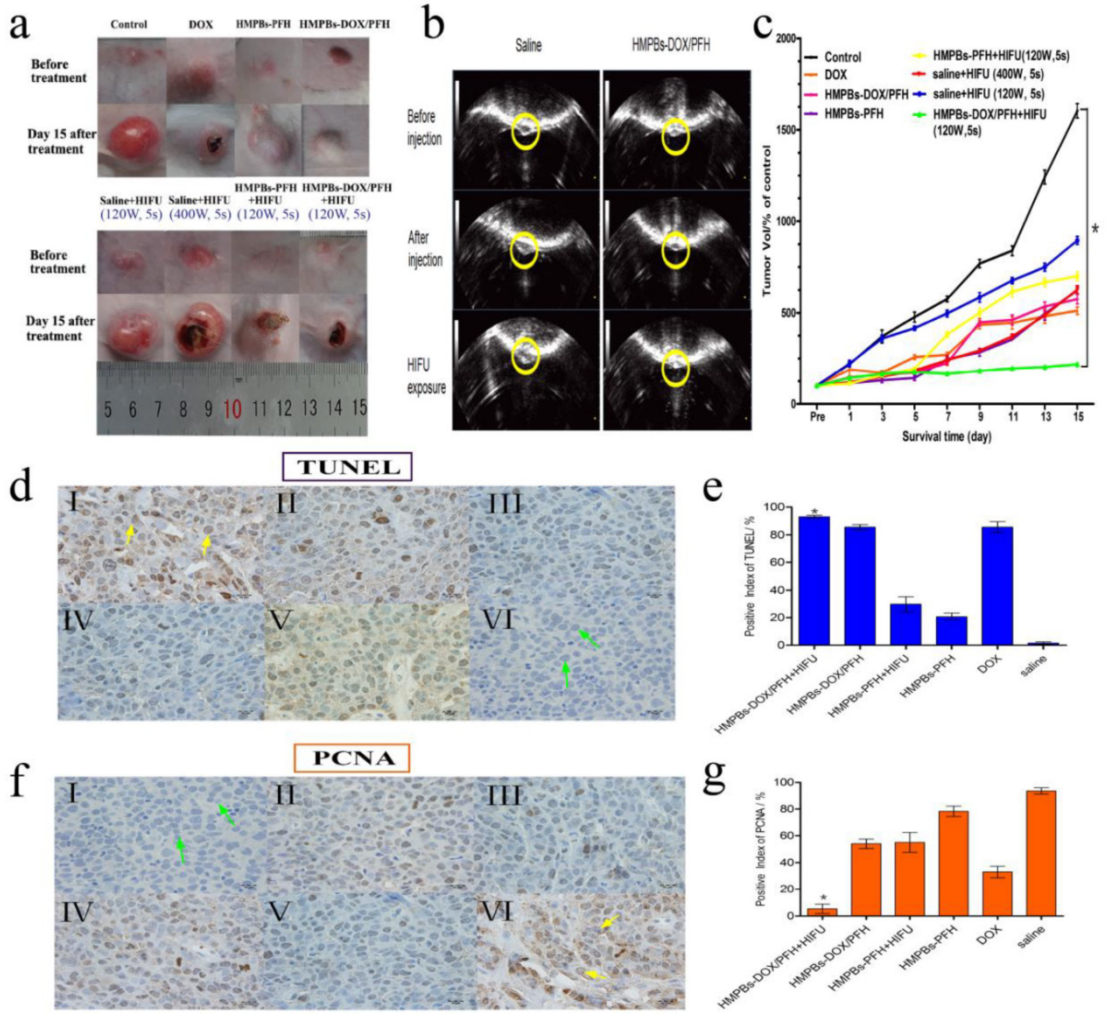

Figure 6. In vivo synergistic HIFU breast cancer surgery. (a) Digital photos of VX_2 tumor loaded rabbits before and day 15 after treatment with different treatments. **(b)** Typical in vivo B-mode ultrasonic images of rabbit VX2 xenograft tumors after injecting 0.2 mL of 6 mg/mL saline control and HMPBs-DOX/PFH before injection (top) and with the subsequent HIFU exposure at 120 W for 5 s (bottom) via intra-tumor injection. The echogenic changes of tumor before and after the ablation were marked by dotted lines, respectively. **(c)** Tumor volume change of rabbits (n = 6) bearing VX_2 treated with different treatments. The tumor volume of control in HMPBs-DOX/PFH +HIFU group (168.2 ± 7.55 %) was apparently lower than that in other groups (e.g., saline: 1603.313 ± 67.261 %) after 15 days observation. **(d)** The expression of TUNEL in tumor tissue by immunohistochemical examination. The nucleus appears brown (yellow arrow in Ⅰ) was TUNEL-positive cell, blue was negative (green arrow in Ⅵ). (Ⅰ) HMPBs-DOX/PFH + HIFU; (Ⅱ) HMPBs-DOX/PFH; (Ⅲ) HMPBs-PFH + HIFU; (Ⅳ) HMPBs-PFH; (Ⅴ) DOX; (Ⅵ) saline. **(e)** The PI of TUNEL in HMPBs-DOX/PFH + HIFU group was higher than that in the other three groups ($p<0.05$). However, there is no significant difference for HMPBs-DOX/PFH + HIFU group to DOX and HMPBs-DOX/PFH group ($p>0.05$) **(f)** The immunohistochemical examination images of PCNA in tumor tissue. The nucleus appears blue (green arrow in Ⅰ) was PCNA-negative cell, brown was positive (yellow arrow in Ⅵ). (Ⅰ) HMPBs-DOX/PFH + HIFU; (Ⅱ) HMPBs-DOX/PFH; (Ⅲ) HMPBs-PFH + HIFU; (Ⅳ) HMPBs-PFH; (Ⅴ) DOX; (Ⅵ) saline. **(g)** The PI of PCNA in the presence of HMPBs-DOX/PFH + HIFU group was lower than that of other five groups ($p<0.05$).

The anti-tumor effect of HMPBs-DOX/PFH was assessed by immunohistochemical methods using the VX_2 xenograft model. Cell apoptosis in tissue sections was evaluated using the TUNEL assay, in which apoptotic cells show brown nuclear staining (Figure 6d). In contrast to the proliferation assay, the positive index (PI) of TUNEL for the HMPB-DOX/PFH + HIFU group was higher than in the other 3 groups ($p<0.05$). However, there was no significant difference for HMPBs-DOX/PFH + HIFU group to DOX and HMPBs-DOX/PFH group ($p>0.05$) (Figure 6e). In the HMPB-DOX/PFH + HIFU group, the expression of PCNAs was absent or reduced, while the other groups were positive for PCNA expression (Figure 6f). Besides, as shown in Figure 6g, the PI of PCNA in the HMPB-DOX/PFH + HIFU group was lower than those of the other 5 groups ($p<0.05$). These results demonstrate that HMPBs-DOX/PFH can be developed as a highly promising HIFU SAs to increase the effectiveness of HIFU therapy and chemotherapy, to enhance tumor ablation efficacy and to improve the apoptosis of cancer cells. HIFU/chemo-synergistic therapy with high therapeutic efficacy may not only lead to tumor ablation but also significantly enhance the sensitivity of tumor chemotherapeutics. Simultaneously, it may reduce the systemic side effects of chemotherapy compared to solo therapy, which can be used to site-specifically treat the residual tumor following the HIFU ablation therapy.

4. Conclusion

We have designed a smart multifunctional theranostic nanoplatform, HMPBs encapsulating DOX and PFH, to achieve in vivo synergistic effects of HIFU/chemotherapy. The unique hollow mesoporous structure endows the nanoplatform with an extraordinarily high loading capacity for phase-transitional PFH and DOX. When stimulated by HIFU, PFH bubbles released via the mesoporous channels of the HMPB shell could alter the acoustic environment and induce the cavitation effect thereby enhancing the performance of US imaging and HIFU therapy. The drug-loading capacity was also dramatically improved, most notably at lower pH values (e.g., tumor sites) and/or focused ultrasound exposure. This characteristic is beneficial for enhancing local antitumor efficiency and avoiding the systemic side effects of chemotherapy. The multifunctional HMPBs-DOX/PFH is expected to increase therapeutic efficacy and accelerate translation to the clinic. This nanoplatform enhanced the intensity of PA images in our study when exposed to HIFU. Whether this feature is valuable for monitoring the therapeutic process in real-time and evaluating residual tumors after HIFU ablation therapy needs further investigation.

Abbreviations

HIFU: High-intensity focused ultrasound; FUS: focused ultrasound; PA: photoacoustic; SAs: synergistic agents; NIR: near-infrared; FDA: Food and Drug Administration; Prussian Blue: PB; PBNPs: PB nanoparticles; MPBs: mesoporous Prussian blue nanoparticles; HMPBs: hollow mesoporous PB nanoparticles; MRI: magnetic resonance imaging; US: ultrasound; CEUS: contrast-enhanced ultrasound; PFH: perfluorohexane; HMPBs-DOX/PFH: hollow mesoporous PB nanoparticles loading perfluorohexane and doxorubicin; PVP: Polyvinylpyrrolidone; UV-Vis: Ultraviolet visible; HCl: hydrochloric acid; PBS: phosphate-buffered saline; TEM: Transmission Electron Microscope; HPLC: high-performance liquid chromatography; MTT: 3-(4,5-dimethyl-2-thiazolyl)-2,5-diphenyl-2-H-tetrazolium bromide; DMSO: dimethylsulfoxide; HE: Hematoxylin and eosin; TUNEL: deoxynucleotidyl transferase-mediated dUTP-biotin nick end-labeling assay; PCNA: proliferating cell nuclear antigen; PI: positive index.

Supplementary Material

Figures S1-S6. http://www.thno.org/v06p0404s1.pdf

Acknowledgments

The authors are grateful to Dr. Jianxin Liu and Bing Liang for assistance with the US and PA imaging and to Qi Wang for technical support with HIFU. This work was supported by the National Natural Science Foundation of China (Grant No.81130025, 81227801), the National Research Program of China (973 Program, Grant No.2011CB707905), China National Funds for Distinguished Young Scientists (51225202) and the China National Fund for Distinguished Young Scientists (51225202).

Competing Interests

The authors have no competing interests.

References

1. Kennedy JE, et al. High-intensity focused ultrasound in the treatment of solid tumours. Nat Rev Cancer. 2005; 5: 321-327.
2. Illing RO, Kennedy JE, Wu F, et al. The safety and feasibility of extracorporeal high-intensity focused ultrasound (HIFU) for the treatment of liver and kidney tumours in a Western population. Br J Cancer. 2005; 93 (8): 890-895.
3. Wu F, Wang ZB, Zhu H, et al. Feasibility of US-guided High-Intensity Focused Ultrasound Treatment in Patients with Advanced Pancreatic Cancer: Initial Experience. Radiology. 2005; 236 (3): 1034-1040.
4. Schmitz AC, Gianfelice D, Daniel BL, et al. Image-guided focused ultrasound ablation of breast cancer: current status, challenges, and future directions. Eur Radiol. 2008; 18 (7): 1431-1441.
5. Huber PE, Jenne JW, Rastert R, et al. A New Noninvasive Approach in Breast Cancer Therapy Using Magnetic Resonance Imaging-guided Focused Ultrasound Surgery. Cancer Res. 2001; 61 (23): 8441-8447.
6. Foley JL, Little JW, Starr FL, et al. Image-guided HIFU neurolysis of peripheral nerves to treat spasticity and pain. Ultrasound Med Biol. 2004; 30 (9): 1199-1207.
7. Harvey CJ, Pilcher JM, Eckersley RJ, et al. Advances in Ultrasound. Clin Radiol. 2002; 57: 157-177.
8. Vaezy S, Shi X, Martin RW, et al. Real-Time Visualzation of High-Intensity Focused Ultrasound Treatment Using Ultrasound Imaging. Ultrasound Med Biol. 2001; 27 (1): 33-42.
9. Wu F, Wang ZB, Chen WZ, et al. Extracorporeal high intensity focused ultrasound ablation in the treatment of 1038 patients with solid carcinomas in China: an overview. Ultrason Sonochem. 2004; 11 (3-4): 149-154.
10. Li YY, Sha WH, Zhou YJ, et al. Short and long term efficacy of high intensity focused ultrasound therapy for advanced hepatocellular carcinoma. J Gastroenterol Hepatol. 2007; 22 (12): 2148-2154.
11. Xu M, Wang LV. Photoacoustic imaging in biomedicine. Rev Sci Instrum. 2006; 77 (4): 041101. doi: 10.1063/1.2195024.
12. Wilson K, Homan K, Emelianov S. Biomedical photoacoustics beyond thermal expansion using triggered nanodroplet vaporization for contrast-enhanced imaging. Nat Commun. 2012; 3: 618.
13. Louie A. Multimodality Imaging Probes: Design and Challenges. Chem Rev. 2010; 110 (5): 3146-3195.
14. Cai W, Chen X. Multimodality molecular imaging of tumor angiogenesis. J Nucl Med. 2008; 49: 113S-128S.
15. Culver J, Akers W, Achilefu S. Multimodality molecular imaging with combined optical and SPECT/PET modalities. J Nucl Med. 2008; 49 (2): 169-172.
16. Wang X, Chen H, Chen Y, et al. Perfluorohexane-encapsulated mesoporous silica nanocapsules as enhancement agents for highly efficient high intensity focused ultrasound (HIFU). Adv Mater. 2012; 24(6): 785-791.
17. Kaneko Y, Maruyama T, Takegami K, et al. Use of a microbubble agent to increase the effects of high intensity focused ultrasound on liver tissue. Eur Radiol. 2005; 15 (7): 1415-1420.
18. Rouffiac V, Duret JS, Peronneau P, et al. Combination of HIFU therapy with contrast-enhanced sonography for quantitative assessment of therapeutic efficiency on tumor grafted mice. Ultrasound Med Biol. 2006; 32 (5): 729-740.
19. Oeffinger BE, Wheatley MA. Development and characterization of a nano-scale contrast agent. Ultrasonics. 2004; 42 (1-9): 343-347.
20. Zhang J, Coulston RJ, Jones ST, et al. One-step fabrication of supramolecular microcapsules from microfluidic droplets. Science. 2012; 335 (6069): 690-694.
21. Moyer LC, Timbie KF, Sheeran PS, et al. High-intensity focused ultrasound ablation enhancement in vivo via phase-shift nanodroplets compared to microbubbles. J Ther Ultrasound. 2015; 3:7. doi: 10.1186/s40349-015-0029-4. eCollection 2015.
22. Wang X, Chen H, Zheng Y, et al. Au-nanoparticle coated mesoporous silica nanocapsule-based multifunctional platform for ultrasound mediated imaging, cytoclasis and tumor ablation. Biomaterials. 2013; 34 (8): 2057-2068.
23. Chen Y, Chen H, Shi J. In vivo bio-safety evaluations and diagnostic/therapeutic applications of chemically designed mesoporous silica nanoparticles. Adv Mater. 2013; 25 (23): 3144-3176.
24. Niu D, Wang X, Li Y, et al. Facile synthesis of magnetite/perfluorocarbon co-loaded organic/inorganic hybrid vesicles for dual-modality ultra-

sound/magnetic resonance imaging and imaging-guided high-intensity focused ultrasound ablation. Adv Mater. 2013; 25 (19): 2686-2692.
25. Li Y, Lin TY, Luo Y, et al. A smart and versatile theranostic nanomedicine platform based on nanoporphyrin. Nat Commun. 2014; 5: 4712. doi: 10.1038/ncomms5712.
26. Cheng Z, Al Zaki A, Hui JZ, et al. Multifunctional nanoparticles: cost versus benefit of adding targeting and imaging capabilities. Science. 2012; 338 (6109): 903-910.
27. Fiorito PA, Goncales VR, Ponzio EA, et al. Synthesis, characterization and immobilization of Prussian blue nanoparticles. A potential tool for biosensing devices. Chem commun (Camb). 2005; 21 (3): 366-368.
28. Liang X, Deng Z, Jing L, et al. Prussian blue nanoparticles operate as a contrast agent for enhanced photoacoustic imaging. Chem Commun (Camb). 2013; 49 (94): 11029-11031.
29. Cai XJ, Jia XQ, Gao W, et al. A Versatile Nanotheranostic Agent for Efficient Dual-Mode Imaging Guided Synergistic Chemo-Thermal Tumor Therapy. Adv Funct Mater. 2015; 25(17): 2520–2529.
30. Li W, Cai X, Kim C, et al. Gold nanocages covered with thermally-responsive polymers for controlled release by high-intensity focused ultrasound. Nanoscale. 2011; 3(4):1724-1730.
31. [31] Kagan D, Benchimol MJ, Claussen JC, et al. Acoustic droplet vaporization and propulsion of perfluorocarbon-loaded microbullets for targeted tissue penetration and deformation. Angew Chem Int Ed Engl. 2012 Jul 23; 51(30):7519-7522.
32. Siegel RA, Rathbone MJ. Overview of Controlled Release Mechanisms. Fundamentals and Applications of Controlled Release Drug Delivery, Advances in Delivery Science and Technology, Controlled Release Society. Springer-Verlag New York Inc.; 2012.
33. Javid A, Ahmadian S, Saboury AA, et al. Chitosan-coated superparamagnetic iron oxide nanoparticles for doxorubicin delivery: synthesis and anticancer effect against human ovarian cancer cells. Chem Biol Drug Des. 2013; 82: 296–306.
34. Unsoy G, Khodadust R, Yalcin S, et al. Synthesis of doxorubicin loaded magnetic chitosan nanoparticles for pH responsive targeted drug delivery. Eur J Pharm Sci. 2014; 62: 243–250.
35. Frenkel V. Ultrasound mediated delivery of drugs and genes to solid tumors. Adv Drug Deliv Rev. 2008; 60(10):1193-1208.
36. Mura S, Nicolas J, Couvreur P. Stimuli-responsive nanocarriers for drug delivery. Nat Mater. 2013; 12: 991-1003.
37. Coussios CC, Farny CH, Haar GT, Roy RA. Role of acoustic cavitation in the delivery and monitoring of cancer treatment by high-intensity focused ultrasound (HIFU). Int J Hyperthermia. 2007; 23(2):105-120.